Free Radical Research, May 2009; 43(5): 457–469

informa
healthcare

Thermal generation of stable $SO_4^{\bullet -}$ spin trap adducts with super-hyperfine structure in their EPR spectra: An alternative EPR spin trapping assay for radical scavenging capacity determination in dimethylsulphoxide

MICHAL ZALIBERA[1], PETER RAPTA[1], ANDREJ STAŠKO[1], LUCIA BRINDZOVÁ[2], & VLASTA BREZOVÁ[1]

[1]*Institute of Physical Chemistry and Chemical Physics, and* [2]*Institute of Biochemistry, Nutrition and Health Protection, Faculty of Chemical and Food Technology, Slovak University of Technology in Bratislava, Radlinského 9, SK-812 37 Bratislava, Slovak Republic*

(Received 24 November 2008; revised 18 February 2009)

Abstract
Thermal decomposition of potassium persulphate ($K_2S_2O_8$) was studied in detail by the EPR spin trapping technique in dimethylsulphoxide (DMSO), employing 5,5-dimethyl-1-pyrroline-N-oxide (DMPO), 5-ethoxycarbonyl-5-methyl-1-pyrroline-N-oxide (EMPO) and 5-(diisopropoxyphosphoryl)-5-methyl-1-pyrroline-N-oxide (DIPPMPO) as spin traps. DMPO and/or its derivatives exclusively trapped the primary formed $SO_4^{\bullet -}$ radical anions producing stable spin adducts with half-lives exceeding 2 h at room temperature. High-resolution EPR spectra of these adducts showed unusually rich hyperfine structure due to the interaction of the unpaired electron with all magnetically active nuclei of the spin trap moiety. In contrast to aprotic DMSO solvent, $^{\bullet}$DMPO-OH adducts dominated in mixed DMSO/water solutions with water content higher than 50%. The thermal decomposition of $K_2S_2O_8$ in DMSO represents an effective source of free radicals for the radical scavenging capacity (RSC) determination assay, applicable to hydrophilic as well as hydrophobic antioxidants. Efficiency of the assay is demonstrated with a series of cereal samples.

Keywords: *EPR spectroscopy, spin trapping, DMSO, sulphate radical anion, antioxidant.*

Abbreviations: *ACN, acetonitrile; BHT, 2,6-di-tert-butyl-4-methyl-phenol; DEPMPO, 5-diethoxyphosphoryl-5-methyl-1-pyrroline N-oxide; DIPPMPO, 5-(diisopropoxyphosphoryl)-5-methyl-1-pyrroline-N-oxide; DMF, N,N-dimethylformamide; DMPO, 5,5-dimethyl-1-pyrroline-N-oxide; DMSO, dimethylsulphoxide; EMPO, 5-ethoxycarbonyl-5-methyl-1-pyrroline-N-oxide; hfcs, hyperfine coupling constants; r, correlation coefficient; RSC, radical scavenging capacity; TEAC, Trolox equivalent antioxidant capacity; Trolox, 6-hydroxy-2,5,7,8-tetramethylchroman-2-carboxylic acid.*

Introduction

The persulphate or peroxodisulphate anion ($S_2O_8^{2-}$) is an effective oxidant used in the organic synthesis as well as other areas of chemical and biochemical research. The homolytic scission of the peroxo (O-O) bond in $S_2O_8^{2-}$ by thermolysis [1,2], photolysis [3,4], pulse radiolysis [5,6] or other techniques, generates the sulphate radical anion ($SO_4^{\bullet -}$), a reactive oxygen-centred radical with a high value of reduction potential [7]. Previously, a series of studies was published by Davies and Gilbert, where they successfully used the sulphate radicals for oxidation of various sulphides and sulphoxides [8], alkenes and dienes [9], carboxylic acids [10], phenyl substituted carboxylic acid [11] and

Correspondence: Vlasta Brezová, Institute of Physical Chemistry and Chemical Physics, Faculty of Chemical and Food Technology, Slovak University of Technology in Bratislava, Radlinského 9, SK-812 37 Bratislava, Slovak Republic. Tel: ++4212 5932 5666. Fax: ++4212 5292 6032. Email: vlasta.brezova@stuba.sk

ISSN 1071-5762 print/ISSN 1029-2470 online
DOI: 10.1080/10715760902846140

carbohydrates [12]. The reaction with $SO_4^{\bullet-}$ usually yielded a substrate-derived radical that could be consequently characterized by the EPR spectroscopy. In other reports, the attention was focused on the one electron transfer from the $SO_4^{\bullet-}$ to the biological important structures such as DNA, 2'-deoxy adenosine, purine [13], guanosine [13,14], 1,3-dimethyluracil [15,16], cytosine [17], cytidine [18] and pyrimidines [19–22]. Furthermore, it was shown in our laboratory that the process of ageing in drink or food samples can be successfully simulated with the behaviour of *in situ* generated sulphate radicals [23,24]. In this context, the thermal decomposition of $K_2S_2O_8$ was investigated in detail by the EPR spin trapping technique in water and water/ethanol solutions using DMPO [25]. The main signal detected in water solutions was attributed to the hydroxyl radical adduct with DMPO spin trap, but in the mixed water/ethanol solutions the portion of the carbon-centred radical adducts increased with the rising ethanol content. It may be noted that, in the early stages of the $K_2S_2O_8$ decomposition in aqueous media, spectrum of the $^{\bullet}$DMPO-SO_4^{-} adduct could be recognized, but due to its limited stability this signal was not clearly evident later. Indeed, it was proved earlier, by Davies et al. [26], that the $^{\bullet}$DMPO-SO_4^{-} adduct is unstable in water and hydrolyses to finally form the $^{\bullet}$DMPO-OH adduct.

Although the spin trapping of the sulphate radical anion is quite well described in water and characteristic spectra are known for adducts of DMPO [26], as well as its analogue 5-diethoxyphosphoryl-5-methyl-1-pyrroline N-oxide (DEPMPO) [27], the reports on experiments with other solvents are relatively scarce. This reflects a great interest that is nowadays focused on the free radical chemistry in biological systems, and therefore water environment, and the effort to extend the spin trapping method for the use *in vivo*. Actually, Timmins et al. [28] described the generation of the $^{\bullet}$DEPMPO-OH adducts by the nucleophilic substitution of the $SO_4^{\bullet-}$ adducts formed *in vivo*, in mice treated with $FeSO_4{\cdot}7H_2O$ and potassium peroxymonosulphate ($KHSO_5$).

In our previous studies devoted to the antioxidant properties of yeasts [29] and various cereals [30,31] we have extensively used DMSO as the solvent for extraction of ingredients possessing antioxidant effects. The main advantage of DMSO was its ability to dissolve polar as well as non-polar compounds. Consequently, both hydrophilic and lipophilic antioxidants could be extracted into one medium, and a more complex view on the antioxidant properties of the analysed substrates could be obtained. On the other hand, application of DMSO in the EPR spin trapping assays is often complicated by its reactions with reactive radicals, especially hydroxyl radicals [32]. Consequently, an alternative source of reactive oxidant radicals was required for experiments in DMSO solutions. The thermal decomposition of $K_2S_2O_8$ in combination with the spin trapping by DMPO detected by EPR has proved to be a suitable method for our purpose. The generated sulphate radical anion, even thought rather artificial for biology, is a reactive species and its high reduction potential exceeds [33] and reactivity approaches that of the hydroxyl radical, the most important radical oxidant in living systems. Moreover, the thermal decomposition of $K_2S_2O_8$ allowed us to tune the rate of radical formation by the proper choice and control of the experimental temperature. The detail description of the method as well as analysis of the obtained EPR spectra is reported in the paragraphs below.

Materials and methods

Materials

$K_2S_2O_8$ (analytical grade, $\leq 0.001\%$ N), $KHSO_5$ in the form of triple salt $2\,KHSO_5.KHSO_4.K_2SO_4$ (for synthesis) and dimethyl sulphoxide (DMSO, SeccoSolv® max. 0.025% H_2O) were obtained from Merck (Germany). Acetonitrile (ACN) and N,N-dimethylformamide (DMF), both of the p.a. 99.5% GC purity, were acquired from Fluka (Germany). 5,5-Dimethyl-1-pyrroline-N-oxide (DMPO, $\geq$ 97% GC, Sigma-Aldrich, USA) was vacuum distilled and stored at -18°C prior to use. 5-Ethoxycarbonyl-5-methyl-1-pyrroline-N-oxide (EMPO, $\geq$ 95 %) and 5-(diisopropoxyphosphoryl)-5-methyl-1-pyrroline-N-oxide (DIPPMPO, $\geq$ 98 %) from Alexis (Switzerland) were used as received. The following substances from Sigma-Aldrich with declared purities were applied as antioxidants: Trolox (6-hydroxy-2,5,7,8-tetramethylchroman-2-carboxylic acid), BHT (2,6-di-*tert*-butyl-4-methyl-phenol) 97%; gallic acid monohydrate (3,4,5-tri-hydroxy-benzoic acid) 98%; vanillic acid (4-hydroxy-3-methoxybenzoic acid) 97%; syringic acid (4-hydroxy-3,5-dimethoxybenzoic acid) 95%; ferulic acid (*trans*-4-hydroxy-3-methoxy-cinnamic acid) 99%; caffeic acid (*trans*-3,4-dihydroxycinnamic acid) 98%; *p*-coumaric acid (*trans*-4-hydr oxycinnamic acid) 98%; 3,4-dihydroxybenzoic acid 98%. Ethanol of spectroscopic grade was obtained from Microchem (Slovak Republic) and H_2O_2, $FeSO_4{\cdot}7H_2O$, K_2HPO_4, $NaH_2PO_4{\cdot}12H_2O$, H_2SO_4 of analytical grade were purchased from Lachema (Czech Republic). Distilled and deionized water was used for preparation of solutions where required.

EPR measurements and their evaluations

All EPR measurements were carried out in a single 4 mm flat quartz cell in a Bruker TE_{102} (ER 4102 ST) cavity using the Bruker EMX or the Adani CMS 8400 portable EPR spectrometers working in the X-band. The ER 4111 VT temperature unit (Bruker,

Germany) was used for temperature regulation. Special attention was focused to the identical positioning of the cell in the EPR cavity and the proper spectrometer tunning in all experiments. The stop flow experiment was performed with the assembly described in Staško et al. [34] attached to the 4 mm flat quartz cell. Unless otherwise stated in the text, the spectrometer settings were (i) microwave power, 10 mW; field modulation, 0.1 mT; conversion time, 20.48 ms; time constant, 81.92 ms; resolution, 1024 points for experiments under air and quantitative EPR spectra and (ii) microwave power, 1 mW; field modulation, 0.005 mT; conversion time, 40.96 ms; time constant, 10.24 ms; resolution, 4096 points for high-resolution experiments under argon. Typical reaction mixture contained 1 mM $K_2S_2O_8$ and 20 mM DMPO, EMPO or DIPPMPO in DMSO and/or DMSO, ACN/water mixtures (v/v; volume ratio) as stated in the text. Solution of 1 mM $K_2S_2O_8$ and 80 mM DMPO was used in DMF. The Fenton system for hydroxyl radicals generation consisted of 1 mM $FeSO_4$, 0.1 mM H_2SO_4 and 1 mM H_2O_2 in the phosphate buffer pH = 7. Detected EPR spectra were analysed and simulated by the Bruker software WinEPR and SimFonia and the Winsim2002 software free available from the website of National Institute of Environmental Health Sciences (NIEHS) (http://epr.niehs.nih.gov/) [35].

Preparation of cereal extracts

The cereal grains cultivation conditions as well as procedures for the extracts preparation were identical to those previously described in detail [30,31]. Briefly, 1 g of defatted whole grain flour was extracted with 65% ethanol (3×15 ml) at 80°C for 1 h. Extracts were filtrated and the supernatants collected, combined and dried in vacuum at 40°C. Residues containing extracted antioxidants were dissolved in 5 ml DMSO.

Results and discussion

Identification of the $^{\bullet}$DMPO-SO_4^- adduct

Figure 1 shows the time course of integral intensities of EPR spectra (I_{EPR}) detected in the air-saturated solution of 1 mM $K_2S_2O_8$ and 20 mM DMPO in DMSO at 333 K. Intensity of a six-line EPR signal (Figure 2A) with hyperfine coupling constants (hfcs) $a_N = 1.292$ mT, $a_H^{\beta} = 0.922$ mT, $a_H^{\gamma} = 0.138$ mT, $a_H^{\gamma} = 0.063$ mT characteristic for an oxygen-centred radical adduct, was continually increasing during the first 40 min of the experiment. The decay of the signal in the following minutes could be successfully fitted by a pseudo-first order kinetic curve, providing the half-life of the detected species $t_{1/2} = 20$ min at 333 K. However, at room temperature of 298 K the half-life value increased to $t_{1/2} = 132$ min, pointing to the outstanding stability of the adduct formed. In this stage we could only tentatively assign the detected signal to the DMPO adduct of the $SO_4^{\bullet-}$ radical anion. Nevertheless, the observed hfcs were rather different from those reported for $^{\bullet}$DMPO-SO_4^- in water ($a_N = 1.38$ mT, $a_H^{\beta} = 1.02$ mT, $a_H^{\gamma} = 0.14$ mT, $a_H^{\gamma} = 0.08$ mT) [26]. In order to prove our suggestion we have performed an identical experiment with an alternative source of sulphate radical anions, i.e. potassium peroxymonosulphate. The solution of 1 mM $2KHSO_5.KHSO_4.K_2SO_4$ and 20 mM DMPO in 90% DMSO/water mixture was heated in the cavity of the EPR spectrometer at 333 K and the identical EPR signal as shown in Figure 2A was observed (results not shown). Moreover, an adduct with closely similar coupling constants was detected when the decomposition of $K_2S_2O_8$ was carried out in two other aprotic solvents, namely acetonitrile (ACN) and N,N-dimethylformamide (DMF) (for details see next section). The final proof for $^{\bullet}$DMPO-SO_4^- formation was gained by mixing of the adduct pre-formed in DMSO with a 10-fold excess of water in a stop-flow system [34]. Series of EPR spectra was detected in 30 s intervals, and immediately after mixing a six-line spectrum with hfcs of $a_N = 1.372$ mT, $a_H^{\beta} = 1.014$ mT, $a_H^{\gamma} = 0.140$ mT, $a_H^{\gamma} = 0.075$ mT overlapped with a four-line signal with low intensity and hyperfine couplings $a_N = 1.495$ mT, $a_H^{\beta} = 1.453$ mT was observed (see Supplementary material). The intensity of the first signal decreased with time at the extent of the second one, as expected for the hydrolysis of the $^{\bullet}$DMPO-SO_4^- to $^{\bullet}$DMPO-OH. Indeed the observed coupling constants are consistent with those reported by Davies et al. [26] for the $^{\bullet}$DMPO-SO_4^- ($a_N = 1.38$ mT, $a_H^{\beta} = 1.02$ mT, $a_H^{\gamma} = 0.14$ mT, $a_H^{\gamma} = 0.08$ mT) and $^{\bullet}$DMPO-OH ($a_N = 1.49$ mT, $a_H^{\beta} = 1.49$ mT), respectively. The slight differences can be ascribed to the effect of different polarity of our solvent mixture.

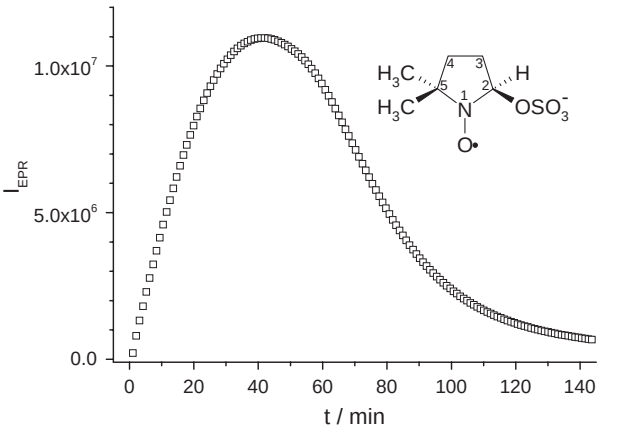

Figure 1. The time course of EPR integral intensities (I_{EPR}) obtained for the $^{\bullet}$DMPO-SO_4^- adduct signal in air-saturated 1 mM $K_2S_2O_8$, 20 mM DMPO solution in DMSO at 333 K: microwave power, 10 mW; field modulation, 0.1 mT. Inset shows the structure of the $^{\bullet}$DMPO-SO_4^- adduct with the corresponding atom numbering. For individual EPR spectrum see Figure 2A.

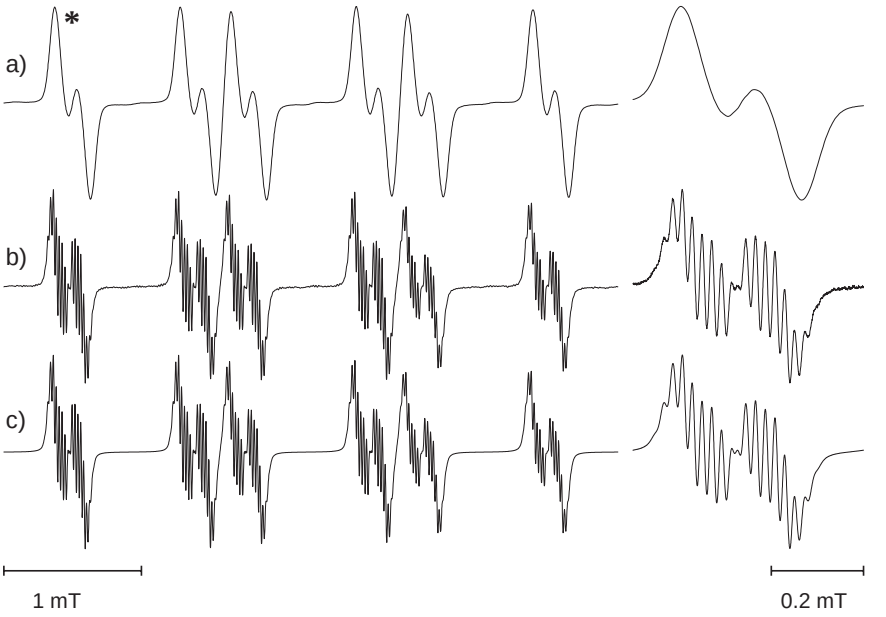

Figure 2. EPR spectrum of the $^{\bullet}$DMPO-SO_4^- adduct obtained for (A) air-saturated 1 mM $K_2S_2O_8$ and 20 mM DMPO in DMSO at 333 K: microwave power, 1 mW; field modulation, 0.02 mT; (B) argon-saturated solution and field modulation, 0.005 mT. (C) Simulation of the spectrum in B by a single species ($r = 0.992$). The low field lines (*) are expanded in the right part and hyperfine coupling constants are listed in Table I.

Via these experiments we were able to prove that a stable $^{\bullet}$DMPO-SO_4^- adduct is formed by the thermal decomposition of persulphate in the DMSO environment.

Super-hyperfine structure in the EPR spectrum of the $^{\bullet}$DMPO-SO_4^- adduct

The experiments mentioned above were performed in air-saturated solutions, where interaction with the paramagnetic molecular oxygen caused broadening of the EPR lines. In order to fully characterize the spectra of $^{\bullet}$DMPO-SO_4^- in DMSO, we have repeated the experiments under inert argon atmosphere. The applied microwave power was also reduced to avoid accidental line broadening by signal saturation effects. Under these conditions a high-resolved EPR spectrum with more than 90 lines was observed (Figure 2B). EPR spectra of the DMPO adducts with such high-resolved hyperfine structure are rather rare in the literature. Eberson and Persson [36] have observed a similarly rich-split signal by the irradiation of benzoic acid in dichloromethane with chloranil and assigned it to the $^{\bullet}$DMPO-OOCPh adduct. They were able to rationalize the observed pattern by taking into account the splitting from two γ-hydrogen nuclei in position 3 and six γ-hydrogen nuclei from both methyl groups in position 5 of the DMPO molecule, in addition to the larger splittings from β-hydrogen in position 2 and nitrogen in N-oxyl group. We have employed an analogous strategy in the simulation of the high-resolved spectrum of $^{\bullet}$DMPO-SO_4^-. The successful simulation required the optimization of coupling constants for all 11 hydrogen nuclei in the DMPO moiety (Figure 2C). The best correspondence ($r = 0.992$) was reached using the parameters reported in Table I. Interestingly, here the hyperfine splitting originating from two hydrogen nuclei in position 4 of the DMPO structure is smaller than the splitting from hydrogens of the two non-equivalent methyl groups.

On the other hand, if these two smallest hydrogen couplings were omitted from the calculation, the high-resolved spectrum of $^{\bullet}$DMPO-SO_4^- could be alternatively simulated as a mixture of two species with approximately equal mutual ratio ($^{\bullet}$DMPO-SO_4^- (1), $^{\bullet}$DMPO-SO_4^- (2) in Table I, italics). This simulation actually showed even better agreement with the detected spectrum ($r = 0.995$). Recently - several papers were published dealing with the line width alternation observed in the spectrum of the $^{\bullet}$DMPO-OOH adduct [37–40] and the line width alternation with additional super-hyperfine splitting in the spectrum of the closely related $^{\bullet}$DEPMPO-OOH [38,39]. In both cases, experiments with the selectively deuterated spin traps were able to prove that the long-range couplings, i.e. couplings from γ-hydrogens, are detected in the spectra [38,40] and in the case of $^{\bullet}$DEPMPO-OOH are responsible for the observed super-hyperfine structure [40]. More important, the asymmetry in the EPR spectra was successfully simulated by considering two conformers of $^{\bullet}$DMPO-OOH [37–39] and two conformers of the main *trans*-$^{\bullet}$DEPMPO-OOH diastereoisomer, respectively [39,40]. Furthermore, the chemical exchange between the two conformers with different coupling constants was evident from the spectra

Table I. Hyperfine coupling constants of the •DMPO-SO_4^-, •DIPPMPO-SO_4^- and •EMPO-SO_4^- adducts at different temperatures in DMSO.

T/K	Adduct	Abundance/%	Hyperfine coupling constants/mT				
			a_N	a_H^β	a_H^γ	$a_{H\,(CH3)}^\gamma$	a_P
333	•DMPO-SO_4^-	100	1.292	0.918	0.137 0.063	0.022 0.020	—
	or				0.017 0.005		
	•DMPO-SO_4^- (1)	*48.7*	*1.292*	*0.918*	*0.156* *0.063*	*0.023* *0.018*	—
	•DMPO-SO_4^- (2)	*51.3*	*1.292*	*0.918*	*0.118* *0.063*	*0.023* *0.018*	—
313	•DMPO-SO_4^-	100	1.285	0.910	0.139 0.065 0.017 0.005	0.023 0.018	—
298	•DMPO-SO_4^-	100	1.279	0.902	0.140 0.067 0.016 0.006	0.024 0.018	—
333	*trans*-•DIPPMPO-SO_4^-	97.5	1.253	0.919	0.096 0.073 0.035 0.022	0.042	4.577
	cis-•DIPPMPO -SO_4^-	2.5	1.285	1.098	0.113 0.054	0.035	3.846
313	*trans*-•DIPPMPO-SO_4^-	97.1	12.47	0.910	0.096 0.075 0.035 0.023	0.043	4.597
	cis-•DIPPMPO -SO_4^-	2.9	1.283	1.098	0.117 0.057	0.036	3.828
298	*trans*-•DIPPMPO-SO_4^-	98.1	1.243	0.903	0.097 0.076 0.036 0.023	0.043	4.613
	cis-•DIPPMPO -SO_4^-	1.9	1.267	1.076	0.127 0.053	0.037	3.809
333	*trans*-•EMPO-SO_4^-	97.8	1.240	0.920	0.114 0.063 0.015 0.005	0.028	—
	cis-•EMPO-SO_4^-	2.2	1.262	1.176	0.067 0.054	0.031	—
313	*trans*-•EMPO-SO_4^-	98.2	1.235	0.915	0.115 0.063 0.016 0.005	0.028	—
	cis-•EMPO-SO_4^-	1.8	1.207	1.285	0.065 0.059	0.030	—
298	*trans*-•EMPO-SO_4^-	97.9	1.230	0.912	0.116 0.064 0.016 0.005	0.028	—
	cis-•EMPO-SO_4^-	2.1	1.216	1.251	0.065 0.055	0.033	—

recorded at varying experimental temperatures [39,40].

In order to distinguish between the two possible interpretations suggested by the simulations, namely presence of a single •DMPO-SO_4^- conformer with EPR spectrum characterized by a coupling to all DMPO hydrogen nuclei or presence of two •DMPO-SO_4^- (1), •DMPO-SO_4^- (2) conformers, we have performed the experiments with our system at three temperatures (298, 313, 333 K), and we were looking for the possible conformer exchange. The solution with 1 mM $K_2S_2O_8$ and 20 mM DMPO in DMSO was incubated under argon atmosphere at 333 K for 20 min, in the EPR cell inside the cavity of

Table II. Hyperfine coupling constants for the DMPO adducts detected after 20 min thermal decomposition of 1 mM $K_2S_2O_8$ in the presence of 20 mM DMPO at 333 K, in solutions with different DMSO, DMF, ACN/water ratios.

			Hyperfine coupling constants/mT			
solvent:H_2O v/v	Adduct	Abundance/%	a_N	a_H^β	a_H^γ	$a_{H\,(CH3)}^\gamma$
DMSO, 1.0	•DMPO-SO_4^-	100	1.292	0.918	0.137	0.022
					0.063	0.020
					0.017	
					0.005	
DMF, 1.0*	*•DMPO-SO_4^-*	*84*	*1.288*	*0.886*	*0.141*	*0.023*
					0.064	*0.019*
					0.021	
					0.005	
	•DMPO-OR	*13*	*1.367*	*1.125*	*0.090*	–
	•DMPO-R	*3*	*1.445*	*1.745*	–	–
ACN, 0.95	*•DMPO-SO_4^-*	*100*	*1.309*	*0.970*	*0.132*	
					0.064	*0.022*
					0.017	*0.018*
					0.003	
DMSO, 0.8	•DMPO-SO_4^-	96	1.308	0.954	0.136	0.022
					0.064	0.018
					0.016	
					0.003	
	•DMPO-OR'	4	1.402	1.230	0.079	–
DMSO, 0.7	•DMPO-SO_4^-	26	1.320	0.971	0.138	–
					0.067	
	•DMPO-OR'	72	1.418	1.248	0.079	–
	•DMPO-R'	2	1.500	2.160	–	–
DMSO, 0.5	•DMPO-OH	100	1.448	1.314	0.074	–
DMSO, 0.3	•DMPO-OH	100	1.471	1.369	0.068	–
DMSO, 0.0	•DMPO-OH	100	1.495	1.433	0.063	–

* 80 mM DMPO.

the spectrometer, and subsequently EPR spectra were recorded at 298, 313 and 333 K, respectively, using the identical instrument settings. No dramatic changes in the spectra were observed with the decreasing temperature (see Supplementary material), the most remarkable being line broadening of the two major high-field lines. This effect could be easily explained by the hindered motion of the adduct molecule due to the increase in the solvent viscosity, and was actually observed in a lower extent already at 333 K as the DMSO is a rather viscous liquid. A small decrease was also observed in the a_N and a_H^β values (see Table I) with the decreasing temperature. However, the a_N and a_H^β couplings decreased in the same manner and this fact is inconsistent with the expected slowing of the conformer exchange. It can be probably assigned to some temperature-related effect on coupling constant. When critically considering the results, this experiment brought no evidence for the presence of two conformers of the •DMPO-SO_4^- adduct and therefore EPR signal was finally assigned to a single •DMPO-SO_4^- conformer characterized by the EPR spectrum with hyperfine splitting from all hydrogen nuclei of the DMPO moiety detected in the DMSO solutions.

The high resolved EPR spectra with super-hyperfine structure were also observed during the thermal decomposition of $K_2S_2O_8$ in ACN and DMF solutions under argon atmosphere. Close similarity of the coupling constants observed in the three different aprotic solvents (DMSO, ACN and DMF—see Table II and Supplementary material) strongly supports the identification of the discussed adduct as the •DMPO-SO_4^-, described already in the previous section. •DMPO-SO_4^- was the only adduct detected in the 95% ACN/water solution (v/v) containing 1 mM $K_2S_2O_8$ and 20 mM DMPO after 20 min incubation at 333 K. However, its yield and stability were lower than in the corresponding dimethylsulphoxide solution. On the other hand, a 4-fold increase of the DMPO concentration was required to produce the •DMPO-SO_4^- as the major adduct in DMF. Additionally, two other DMPO adducts with lower abundance and coupling constants typical for an oxygen (•DMPO-OR) and a carbon-centred (•DMPO-R) radical were detected in the reaction mixture of 1 mM $K_2S_2O_8$, 80 mM DMPO in DMF at 333 K (see Table II). The observed behaviour resembles well the literature data on $SO_4^{\bullet-}$ reactivity in ACN [41,42] and DMF [43].

Trapping of the $SO_4^{\bullet-}$ with EMPO and DIPPMPO

In the last few decades a variety of DMPO derivatives were synthesized and tested for their spin trapping ability (see [44,45] for reviews). The often repeated motivation for their synthesis was the production of a

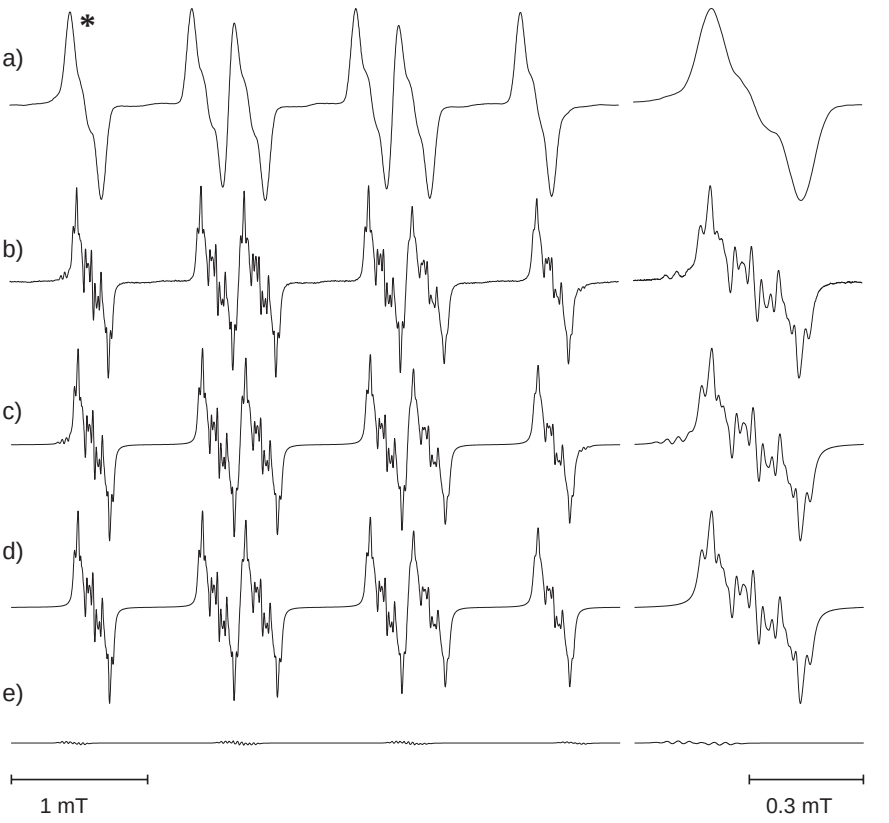

Figure 3. EPR spectrum of the $^{\bullet}$EMPO-SO_4^- adduct obtained for (A) air-saturated 1 mM $K_2S_2O_8$ and 20 mM EMPO in DMSO at 333 K: microwave power, 1 mW; field modulation, 0.02 mT; (B) argon-saturated solution and field modulation, 0.005 mT. (C) Simulation of the spectrum in B; (D) the *trans*-$^{\bullet}$EMPO-SO_4^- simulation; (E) the *cis*-$^{\bullet}$EMPO-SO_4^- diastereoisomer component simulation. The low field lines (*) are expanded in the right part and the hyperfine coupling constants are listed in Table I.

spin trap that would yield a persistent adduct of the biologically important superoxide radical anion without decomposition artefacts, such as the hydroxyl adduct formation. Some of these new agents are now commercially available and we chose EMPO and DIPPMPO for further experiments on the thermal decomposition of potassium persulphate. Both EMPO and DIPPMPO, together with the more popular phosphorylated analogue DEPMPO, belong to the group of derivatives where one of the methyl groups in the DMPO moiety is substituted. The super-hyperfine structure in their EPR spectra should be therefore simplified when compared to DMPO adducts. However, the substitution of the methyl group forms a chiral centre on the 5-carbon and therefore two diastereoisomers can be formed for the EMPO- and/or DIPPMPO-adduct, *cis* or *trans* with respect to the substituent. It has been shown previously that the *cis* and *trans* EMPO, as well as DIPPMPO adducts show different EPR spectra and can be therefore identified in the isomeric mixture [46], nevertheless when more than one radical is formed in the system the obtained signals can be quite difficult to interpret.

Figure 3A and B, Figure 4A and B, show EPR spectra obtained in the air- and argon-saturated solutions of 1 mM $K_2S_2O_8$ and 20 mM EMPO or DIPPMPO in DMSO, respectively, incubated for 20 min at 333 K. Similar to experiments with the DMPO spin trapping agent, intense and stable paramagnetic signals were obtained. Half-lives of the produced species estimated from the decay of their EPR signal were $t_{1/2} = 34$ and 37 min at 333 K and $t_{1/2} = 233$ and 290 min at 298 K for EMPO and DIPPMPO sulphate radical anion adducts, respectively. Analogously as observed in our experiments, literature data demonstrate that adducts of the DMPO derivatives show enhanced stability and most persistent adducts are formed with the phosphorylated DMPO analogues.

With sufficiently low field modulation, rich and well resolved hyperfine structure could be observed also in the EPR spectra of EMPO and DIPPMPO sulphate radical anion adducts (Figures 3B and 4B). If we look closer at the spectrum in Figure 3B, the presence of at least two species is evident already from a short view. The main signal consists of six major lines with an extra super-hyperfine structure. However, at the base of the most high field and low field line an additional signal with much lower intensity can be resolved. Due to the steric reasons addition of the sulphate radical anion is preferred into the *trans* position with respect to the ethoxycarbonyl group of EMPO, and the high intensity signal was therefore assigned to the *trans*- $^{\bullet}$EMPO-SO_4^- adduct

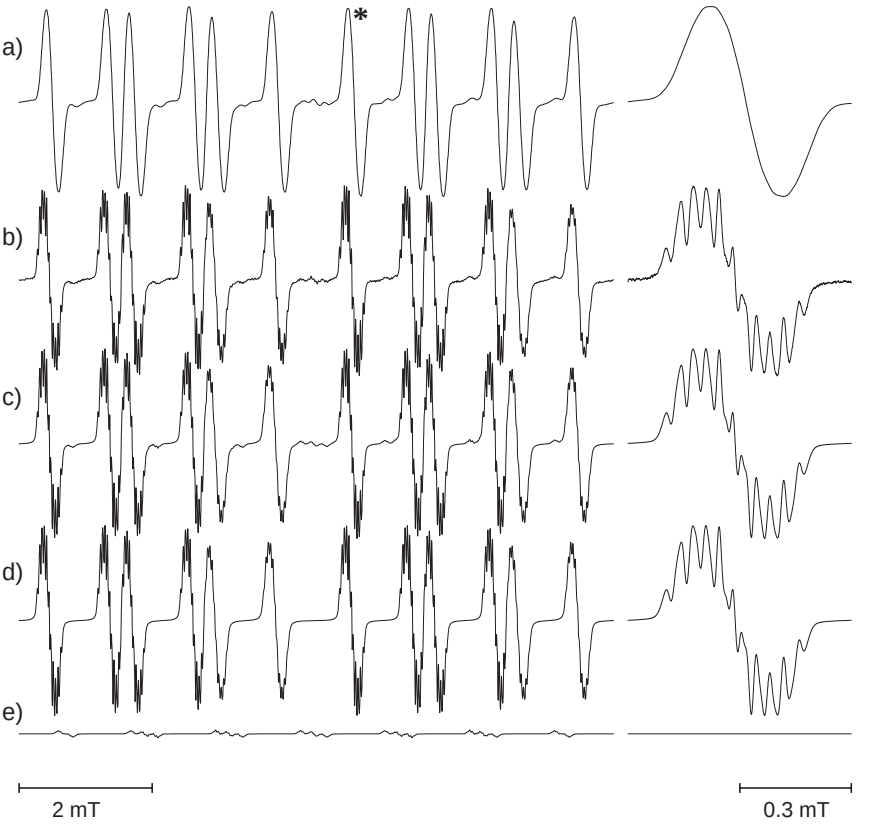

Figure 4. EPR spectrum of the •DIPPMPO-SO_4^- adduct obtained for (A) air-saturated 1 mM $K_2S_2O_8$ and 20 mM DIPPMPO in DMSO at 333 K: microwave power, 1 mW; field modulation, 0.02 mT; (B) argon-saturated solution and field modulation, 0.005 mT. (C) Simulation of the spectrum in B; (D) the *trans*-•DIPPMPO-SO_4^-; (E) the *cis*-•DIPPMPO-SO_4^- diastereoisomer component. The lines marked by (*) are expanded in the right part and the hyperfine coupling constants are listed in Table I.

(Figure 3D). The second one we ascribed to the *cis*-•EMPO-SO_4^-, but because of the low abundance (2%) and severe overlap by the *trans*-•EMPO-SO_4^- signal, the spectral characteristics of this species revealed by the simulation (see Figure 3E and Table I) are rather ambiguous. An analogous situation was observed in the spectrum of •DIPPMPO-SO_4^- (Figure 4B), where the intense 12-line signal with extra super-hyperfine structure is assigned to the *trans*- •DIPPMPO-SO_4^- (Figure 4D) and the second signal with low abundance (2%) to *cis*-•DIPPMPO-SO_4^- adduct (Figure 4E). Simulation of the *trans*-•EMPO-SO_4^- and *trans*-•DIPPMPO-SO_4^- spectra considering a single species provided satisfying fits of the experimental data only if couplings from all hydrogen nuclei in the EMPO and DIPPMPO moieties were optimized. The best agreements ($r = 0.993$ for *trans*-•EMPO-SO_4^- and $r = 0.995$ for *trans*-•DIPPMPO-SO_4^-) were achieved when the a_H^γ values for two hydrogens in position 4 of the EMPO and DIPPMPO moiety were chosen smaller than for the methyl hydrogens (Table I), similar to that found for •DMPO-SO_4^-.

Presence of the possible conformer or diastereoisomer exchange was probed by experiments at three different temperatures (298, 313, 333 K). The spectra obtained for •EMPO-SO_4^- and •DIPPMPO-SO_4^- together with the corresponding computer simulations are available in the Supplementary material and the hyperfine coupling constants (hfcs) are listed in Table I. Similar to by •DMPO-SO_4^-, no dramatic changes in EPR spectra were observed in the investigated temperature range and the small changes in a_N and a_H^β couplings are inconsistent with the conformer or diastereoisomer exchange and were probably caused by some solvent- or temperature-related effects.

Thermal decomposition of potassium persulphate in DMSO/water mixtures

The main purpose of the above-mentioned experiments was the full characterization of an EPR spin trapping system with effective source of reactive radicals in combination with a spin trap yielding persistent radical adducts. The system was aimed for application in analysis of the radical scavenging capacities of various substrates, including biological samples. As biological samples usually contain some amount of water that cannot be always completely removed, we have additionally investigated the thermal decomposition of $K_2S_2O_8$ in various DMSO/water mixtures.

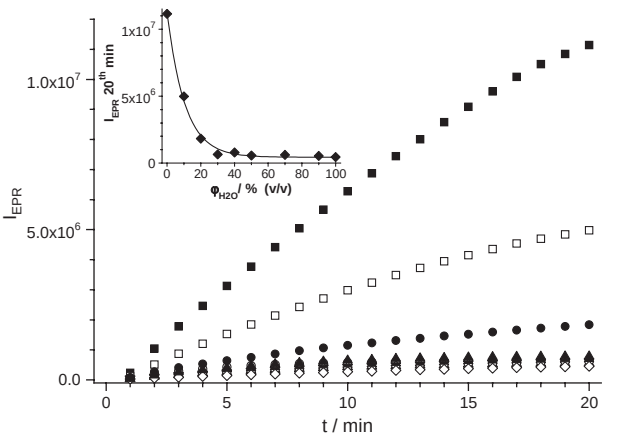

Figure 5. The time course of integral intensities of EPR spectra (I_{EPR}) monitored in 1 mM $K_2S_2O_8$ and 20 mM DMPO argon-saturated solutions with various DMSO/water ratios; ■ 0%, □ 10%, ● 20%, ○ 30%, ▲ 40%, △ 50%, ▼ 60%, ▽ 90%, ◇ 100% of water (v/v) at 333 K (microwave power, 10 mW; field modulation, 0.1 mT). Inset: I_{EPR} in 20th min vs DMSO/water ratio.

The time courses of integral intensities of EPR spectra monitored in 1 mM $K_2S_2O_8$ and 20 mM DMPO argon-saturated solutions with various DMSO/water ratios at 333 K are shown in Figure 5. Significantly lower DMPO adduct yield was achieved when water was added to the reaction system in comparison to the pure DMSO solutions. The inset in Figure 5 shows the nearly exponential decrease in the EPR intensity after 20 min of reaction with the increasing water content. An opposite trend was observed in our previous work where the thermal decomposition of $K_2S_2O_8$ was studied in water/ethanol solutions [25]. There the maximal DMPO adduct yield was detected in pure water solutions and decreased with increasing ethanol content. However, these two systems are not directly comparable, as different radical adducts are formed in water/ethanol and water/DMSO solutions during the thermal decomposition of $K_2S_2O_8$. The dramatic decrease in DMPO adduct formation with only a small increase of water content imposes critical requirements on the purity of the materials used, when reproducible and quantitatively comparable results want to be obtained.

In addition to the changes in the DMPO adduct yield, qualitative changes in the EPR spectra were observed. In other words, different DMPO adducts are formed during the thermal decomposition of $K_2S_2O_8$, depending on the DMSO/water ratio, and are listed in Table II (see also Supplementary material). The $^{\bullet}$DMPO-SO_4^- was the dominant DMPO adduct still in the 80% DMSO/water solution, where its signal constituted 96% of the integral EPR intensity in 20th min. However, the EPR spectrum changed dramatically when the water content was increased by an additional 10%. In 70% DMSO/water the $^{\bullet}$DMPO-SO_4^- content decreased to 26% and a new oxygen-centred radical adduct with EPR spectrum characterized by coupling constants $a_N = 1.418$ mT, $a_H^{\beta} = 1.248$ mT and $a_H^{\gamma} = 0.079$ mT constituted the major portion of the detected signal, with 72% of the total integral intensity in the 20th min. Additionally, signal of a carbon-centred radical adduct (coupling constants $a_N = 1.500$ mT, $a_H^{\beta} = 2.160$) with 2% of the total integral intensity was observed. At even higher water concentration the EPR spectrum of only a single oxygen-centred radical DMPO adduct was detected during the thermal decomposition of $K_2S_2O_8$, however the coupling constant varied significantly with the DMSO/water ratio ($a_N = 1.448$ mT, $a_H^{\beta} = 1.314$ mT, $a_H^{\gamma} = 0.074$ mT for 50%, $a_N = 1.471$ mT, $a_H^{\beta} = 1.369$ mT, $a_H^{\gamma} = 0.068$ mT for 30% and $a_N = 1.495$ mT, $a_H^{\beta} = 1.433$ mT, $a_H^{\gamma} = 0.063$ mT for 0% DMSO, respectively).

A rational suggestion would favour the formation of $^{\bullet}$DMPO-OH adducts with the increasing water content, either by direct trapping of the $^{\bullet}$OH radical formed in the reaction in equation (1) or by the nucleophilic substitution of the $^{\bullet}$DMPO-SO_4^- (equation 2), as already observed [26].

$$SO_4^{\bullet-} + H_2O \rightarrow {}^{\bullet}OH + H^+ + SO_4^{2-} \quad (1)$$

$$^{\bullet}\text{DMPO-}SO_4^- + H_2O \rightarrow {}^{\bullet}\text{DMPO-OH} + H^+ + SO_4^{2-} \quad (2)$$

The $^{\bullet}$DMPO-OH adduct is known to give the characteristic EPR signal with 1:2:2:1 line intensities due to the approximately equal values of hyperfine couplings $a_N \approx a_H^{\beta} \approx 1.49$ mT in water solutions. However, the $^{\bullet}$DMPO-OH spectral characteristics have not been investigated in DMSO/water mixtures and at elevated temperatures. We have therefore prepared the $^{\bullet}$DMPO-OH adduct by the reaction of $^{\bullet}$OH radicals formed in the Fenton reaction system (1 mM $FeSO_4$, 0.1 mM H_2SO_4 and 1 mM H_2O_2 in the phosphate buffer pH = 7) with the DMPO spin trap (20 mM). The characteristic $^{\bullet}$DMPO-OH EPR signal (Figure 6D, $a_N = 1.493$ mT, $a_H^{\beta} = 1.474$ mT), stable for more than 10 min was observed at 298 K under given experimental conditions. When the above described reaction mixture was diluted with DMSO (1:1 v/v) a completely different EPR pattern was detected at 298 K (Figure 6C, $a_N = 1.447$ mT, $a_H^{\beta} = 1.342$ mT, $a_H^{\gamma} = 0.071$ mT).

The observed spectrum is still quite different from that detected for the $K_2S_2O_8$/DMPO system in 50% DMSO at 333 K (Figure 6A). However, when thermal decomposition of $K_2S_2O_8$ is performed in 50% DMSO at 333 K for 20 min and the solution is consequently cooled down to 298 K, the EPR spectrum identical to that produced by Fenton system followed by 1:1 v/v dilution with DMSO was observed (compare Figure 6B and C; $a_N = 1.447$ mT, $a_H^{\beta} = 1.342$ mT, $a_H^{\gamma} = 0.071$ mT). Therefore the EPR signals detected during the thermal decomposition of $K_2S_2O_8$ in DMSO/water mixtures with water content

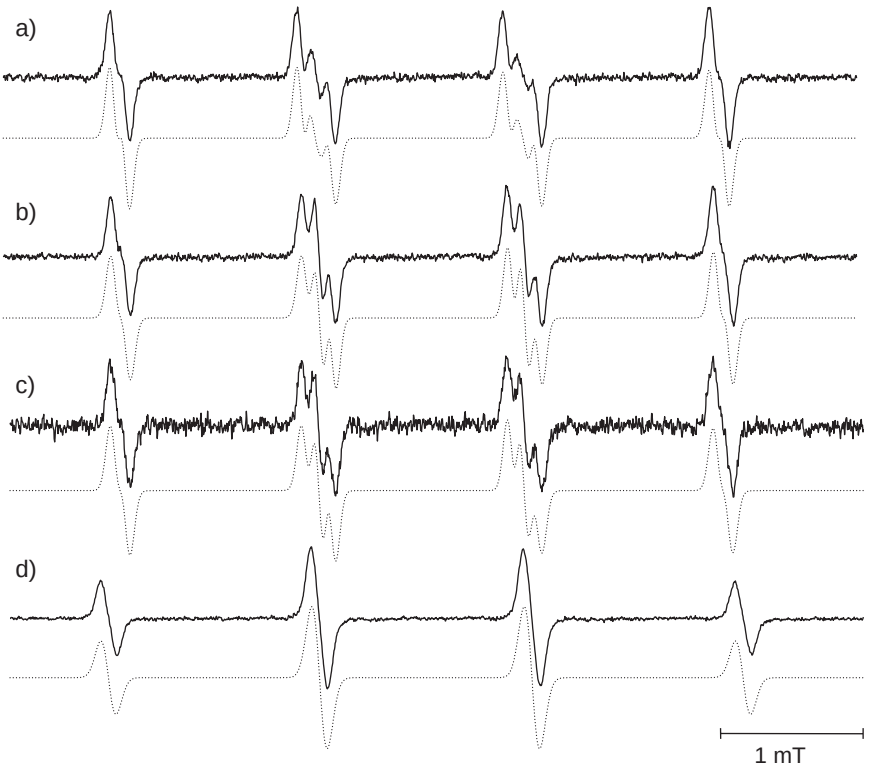

Figure 6. (A) Experimental (solid line) and simulated (dotted line) EPR spectrum of •DMPO-OH obtained in 1 mM $K_2S_2O_8$, 20 mM DMPO argon-saturated solution in 50% DMSO/water after 20 min pre-incubation at 333 K; (B) same as A after cooling to 298 K; (C) EPR spectrum of •DMPO-OH obtained in the Fenton system (1 mM $FeSO_4$, 0.1 mM H_2SO_4 and 1 mM H_2O_2, 20 mM DMPO in the phosphate buffer) after mixing with DMSO 1:1 (v/v) at 298 K; d) EPR spectrum obtained in the Fenton system at 298 K; (microwave power, 10 mW; field modulation, 0.02 mT).

equal or higher than 50% can be attributed to the •DMPO-OH adduct. However, the lower dielectric permittivity of the mixtures, when compared to pure water, as well as increased temperature significantly influence the hyperfine coupling constants and the observed signals largely deviate from the classical 1:2:2:1 line intensity pattern. A tentative assignment of the major signal observed by the thermal decomposition of $K_2S_2O_8$ in 70% DMSO to the •DMPO-OH adduct can also be made by extrapolating the previous observations, nevertheless is rather speculative without additional data.

The EPR spin trapping assay for radical scavenging capacity (RSC) evaluations

One of the techniques, often repeated in antioxidant activity estimation assays, is based on the generation of reactive radicals in the sample with the use of an initiator, while the ability of the sample to terminate these reactive radicals is monitored by various methods [47,48]. The EPR spin trapping technique has one remarkable advantage among other detection methods; it provides qualitative information about the radicals present. The basic idea of an EPR spin trapping assay for RSC evaluation is the monitoring of a competitive reaction between the spin trap and antioxidants present in the sample [49,50]. Using this approach and the $K_2S_2O_8$/DMPO system, the antioxidant activity of wine samples and coffee was previously studied in our group [23,24,50]. In other works we applied the $K_2S_2O_8$/DMPO system to the DMSO extracts from various carotenogenic yeasts [29] and cereals [30,31].

In order to clarify the practical applications of the suggested $K_2S_2O_8$/DMPO/DMSO assay in different systems, the quantitative analysis of the radical scavenging capacity (evaluated in Trolox equivalents) of complex cereal extracts, as well as of the BHT and seven individual phenolic acids, is presented at this point. The time course of integral EPR intensities for the reference sample DMSO (200 μL DMSO, 25 μL 200 mM DMPO in DMSO, 25 μL 10 mM $K_2S_2O_8$ in H_2O) and for six samples containing extract from cereals (200 μL cereal DMSO extract, instead of DMSO in reference sample) recorded at 333 K is shown in Figure 7. The EPR integral intensity in the 20^{th} min, detected for the sample solutions, was compared to that of the reference. The difference between these EPR intensities is proportional to the amount of radicals scavenged by the scavengers present in the corresponding sample. The value for the virtual conditions when all radicals were scavenged was set to 100% of radical scavenging capacity and the RSC of samples is presented as a percentage of radicals scavenged relative to the reference sample

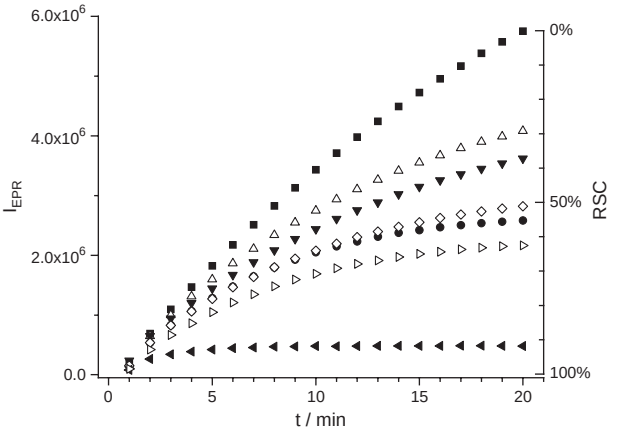

Figure 7. The time course of EPR integral intensities (I_{EPR}) of $^{\bullet}$DMPO-SO_4^- spin adducts observed in air-saturated solutions for the reference system (■ 200 μL DMSO, 25 μL 200 mM DMPO in DMSO, 25 μL 10 mM $K_2S_2O_8$ in H_2O) and in the presence of extracts from cereal and pseudocereal varieties (200 μL cereal extract DMSO solution, 25 μL 200 mM DMPO in DMSO, 25 μL 10 mM $K_2S_2O_8$ in H_2O); △ wheat variety (v.) *Aranka*; ▼ millet v. *Unikum*; ◇ barley v. *Luxor*; ● buckwheat v. *Ballada*; ▷ oat with yellow hulls v. *Triumph*; ◀ oat with black hulls v. *Jostrain*. Right axis illustrates the evaluation of Radical Scavenging Capacity (RSC) as '% of scavenged radicals' after 20 min incubation at 333 K.

representing DMSO solvent. Using this procedure, most of the experimental errors connected with the spectrometer tuning could be avoided. Following the current trends in the antioxidant activity research, we have calibrated the RSC results obtained with $K_2S_2O_8$/DMPO/DMSO to Trolox equivalents, using the calibration curve obtained with DMSO solutions of Trolox (water-soluble α-tocopherol analogue). Results obtained for the studied cereal samples are summarized in Table III.

Concerning the discussion from the previous chapter, at experimental conditions given in Figure 7 (90% DMSO), the $^{\bullet}$DMPO-SO_4^- is the only DMPO adduct formed in the system. Even though its yield is lower than in the pure DMSO, we found that the aqueous $K_2S_2O_8$ are more stable during the storage than the corresponding DMSO solutions (identical results are observed during a week period if stock solution is stored at –18°C). The 90% DMSO/water mixture was therefore used in the experiments for RSC evaluation, where reproducibility is the critical requirement. Moreover, higher modulation amplitude of 0.1 mT was employed in these experiments, in order to facilitate the $^{\bullet}$DMPO-SO_4^- EPR spectra detection, and to achieve improved signal-to-noise ratio. High requirements were also imposed on the purity of the DMSO solvent used, because of the sensitivity of the $^{\bullet}$DMPO-SO_4^- adduct yield to the DMSO/water ratio, and the solvent from a single bottle was applied in all experimental steps.

The $K_2S_2O_8$/DMPO/DMSO system was further tested with the series of seven phenolic acids (vanillic, syringic, 3,4-dihydroxybenzoic, *p*-coumaric, ferulic, caffeic, gallic) and a commercially available synthetic antioxidant BHT; 200 μL of 5 mM sample DMSO solution was used instead of pure DMSO in reference in the assay. The TEAC (Trolox Equivalent Antioxidant Capacity) values, defined as the milimolar concentration of a Trolox solution whose antioxidant capacity is equivalent to a 1.0 mM solution of the substance under study [51], for studied antioxidants are summarized in Table III. Results show that the tested phenolic acids are rather poor scavengers of the $SO_4^{\bullet-}$ radical anion when compared to Trolox, as the most successful among them (gallic acid) showed a 7-times weaker radical scavenging effect than the Trolox standard. This is inconsistent with the observations reported by Rice-Evans et al. [51] for scavenging of the $ABTS^{\bullet+}$ radical cation, where the gallic acid was 2.4-times more effective than Trolox. However, this is not surprising as different mechanisms are probably involved in the scavenging of a stable $ABTS^{\bullet+}$ radical cation and the quite reactive $SO_4^{\bullet-}$ radical anion. On the other hand, synthetic antioxidant BTH has proved to be a quite effective scavenger of $SO_4^{\bullet-}$, even though its activity reaches just half of that of Trolox.

Conclusions

Sulphate anion radicals, $SO_4^{\bullet-}$, are exclusively trapped by DMPO, EMPO and DIPPMPO spin traps during the thermal decomposition of potassium persulphate in DMSO solutions. The $SO_4^{\bullet-}$ adducts formed showed remarkable stability, even at the elevated temperatures. High-resolved EPR spectra of the

Table III. Radical Scavenging Capacity (RSC) evaluated employing the $K_2S_2O_8$/DMPO/DMSO assay at 333 K, expressed as Trolox equivalent antioxidant capacity (TEAC).

Cereal (Variety)	TEAC/mg Trolox/g dry mass	Antioxidant	TEAC/mM Trolox/1 mM sample
Wheat (Aranka)	0.69	Vanillic acid	0.033
Millet (Unikum)	1.13	Syringic acid	0.034
Barley (Luxor)	1.91	3,4-Dihydroxybenzoic acid	0.045
Buckwheat (Ballada)	2.46	*p*-Coumaric acid	0.052
Oat, yellow hulls (Triumph)	3.05	Ferulic acid	0.083
Oat, black hulls (Jostrain)	13.44	Caffeic acid	0.101
		Gallic acid	0.128
		BHT	0.551

•DMPO-SO_4^-, •EMPO-SO_4^- and •DIPPMPO-SO_4^- adducts recorded under argon atmosphere showed unusually rich hyperfine structure. The hyperfine pattern was successfully reconstructed in computer simulations, where long-range couplings for a single species in the case of •DMPO-SO_4^- and two species in the case of •EMPO-SO_4^- and •DIPPMPO-SO_4^- were optimized. Conformational or isomer exchange was not observed in the investigated temperature range (298–333 K). Based on the computer simulations and experiments at different temperatures the existence of a single conformer is proposed for •DMPO-SO_4^- and two diastereoisomers for •EMPO-SO_4^- and •DIPPMPO-SO_4^-. The •DMPO-SO_4^- can be produced as the dominant adduct also in ACN and DMF solvents, however its yield and stability are lower than in the corresponding DMSO solutions.

In contrast to pure DMSO where only $SO_4^{\bullet-}$ adducts were evident, •DMPO-OH adducts dominated in mixed DMSO/water solutions, with water content higher than 50%. However, the lower dielectric permittivity of the mixtures, when compared to pure water, as well as increased temperature, significantly influenced the hyperfine coupling constants and the observed signals largely deviate from the well known 1:2:2:1 line intensity pattern found for •DMPO-OH adduct in aqueous media.

Finally the thermal decomposition of $K_2S_2O_8$ in combination with DMPO spin trapping was introduced as a method for radical scavenging capacity evaluation in DMSO solutions. The procedure for quantification of obtained results was presented and requirements on the suitable reference discussed. The developed assay was further tested with commercially available phenolic acids, as well as natural samples represented by six extracts from cereal and pseudocereal grains. Its advantage among other assays is the applicability to both hydrophilic as well as hydrophobic types of antioxidants. However, results obtained with this system might deviate significantly from other antioxidant activity assays, due to the different nature of the chemistry involved in the independent systems.

Acknowledgements

This work was supported by the Research and Development Agency of the Slovak Republic (contracts No. APVT-20-004504 and APVV-0310-06) and the Scientific Grant Agency of the Slovak Republic (Projects VEGA/1/3579/06, 1/0018/09 and 1/0845/08). The authors thank SCPV, VÚRV Pieštany, VŠS Víglaš-Pstruša (Slovak Republic) for providing the cereal samples.

***Declaration of interest*:** The authors report no conflicts of interest. The authors alone are responsible for the content and writing of the paper.

References

[1] Fenton HJH. LXXIII—Oxidation of tartaric acid in presence of iron. J Chem Soc Perkin Trans 1894;65:899–910.

[2] Fenton HJH, Jackson H. LVI—Crystalline glycollic aldehyde. J Chem Soc Perkin Trans 1899;75:575–579.

[3] Clifton CL, Huie RE. Rate constants for hydrogen abstraction reactions of the sulfate radical, $SO_4^{\bullet-}$ alcohols. Int J Chem Kinet 1989;21:677–687.

[4] Huie RE, Clifton CL. Kinetics of the self-reaction of hydroxymethylperoxyl radicals. Chem Phys Lett 1993;205:163–167.

[5] Elbenberger H, Steenken S, O'Neill P, Schulte-Frohlinde D. Pulse radiolysis and electron spin resonance studies concerning the reaction of $SO_4^{\bullet-}$ with alcohols and ethers in aqueous solution [1]. J Phys Chem 1978;82:749–750.

[6] Heckel E, Henglein A, Beck G. Pulsradiolytische Untersuchung des Radikalanions $SO_4^{\bullet-}$. Ber Bunsenges Phys Chem 1966;70:149–154.

[7] Stanbury DM. Reduction potentials involving inorganic free radicals in aqueous solution. Adv Inorg Chem 1989;33:69–138.

[8] Davies MJ, Gilbert BC, Norman ROC. Electron spin resonance. Part 67. Oxidation of aliphatic sulphides and sulphoxides by the sulphate radical anion ($SO_4^{\bullet-}$) and of aliphatic radicals by the peroxydisulphate anion ($S_2O_8^{2-}$). J Chem Soc Perkin Trans 2 1984;3:503–509.

[9] Davies MJ, Gilbert BC. Electron spin resonance studies. Part 68. Addition versus overall one-electron abstraction in the oxidation of alkenes and dienes by $SO_4^{\bullet-}$, $Cl_2^{\bullet-}$, and •OH in acidic aqueous solution. J Chem Soc Perkin Trans 2 1984;11:1809–1815.

[10] Davies MJ, Gilbert BC, Barry Thomas C, Young J. Electron spin resonance studies. Part 69. Oxidation of some aliphatic carboxylic acids, carboxylate anions, and related compounds by the sulphate radical anion ($SO_4^{\bullet-}$). J Chem Soc Perkin Trans 2 1985;8:1199–1204.

[11] Gilbert BC, Scarratt CJ, Thomas CB, Young J. Electron spin resonance studies. Part 71. Side-chain oxidation pathways in the reactions of •OH and $SO_4^{\bullet-}$ with some phenyl-substituted carboxylic acids, their anions, and some related compounds. J Chem Soc Perkin Trans 2 1987;3:371–380.

[12] Gilbert BC, Lindsay Smith JR, Taylor P, Ward S, Whitwood AC. The interplay of electronic, steric and stereoelectronic effects in hydrogen-atom abstraction reactions of $SO_4^{\bullet-}$, revealed by EPR spectroscopy. J Chem Soc Perkin Trans 2 1999;8:1631–1637.

[13] Steenken S. Purine bases, nucleosides, and nucleotides: Aqueous solution redox chemistry and transformation reactions of their radical cations and e^- and OH adducts. Chem Rev 1989;89:503–520.

[14] Candeias LP, Steenken S. Structure and acid-base properties of one-electron-oxidized deoxyguanosine, guanosine, and 1-methylguanosine. J Am Chem Soc 1989;111:1094–1099.

[15] Schuchmann HP, Deeble DJ, Olbrich G, Von Sonntag C. The $SO_4^{\bullet-}$ induced chain reaction of 1,3-dimethyluracil with peroxodisulphate. Int J Radiat Biol 1987;51:441–453.

[16] Bothe E, Deeble DJ, Lemaire DGE, Rashid R, Schuchmann MN, Schuchmann HP, Schulte-Frohlinde D, Steenken S, Von Sonntag C. Pulse-radiolytic studies on the reactions of $SO_4^{\bullet-}$ with uracil derivatives. Radiat Phys Chem 1990;36:149–154.

[17] Hazra DK, Steenken S. Pattern of OH radical addition to cytosine and 1-, 3-, 5-, and 6-substituted cytosines. Electron transfer and dehydration reactions of the OH adducts. J Am Chem Soc 1983;105:4380–4386.

[18] Niehaus H, Hildenbrand K. Continuous-flow and spin-trapping EPR studies on the reactions of cytidine induced by the sulfate radical-anion in aqueous solution. Evidence for

an intermediate radical-cation. J Chem Soc Perkin Trans 2 2000;5:947–952.
[19] Itahara T, Ebihara R, Seto Y, Fujii Y, Tada M. Reaction of nucleic acids bases and their derivatives with peroxodisulfate ion. Nucleic Acids Symp Ser 1985;16:61–64.
[20] Itahara T, Ide N, Nishino A. Oxidation of pyrimidine bases and their derivatives by sodium peroxodisulfate. Nucleic Acids Symp Ser 1989;21:5–6.
[21] Itahara T, Koga S, Yoshitake T. Oxidation of nucleosides and nucleotides by peroxosulfate ions. Nucleic Acids Symp Ser 1990;22:9–10.
[22] Hildenbrand K. Spin-trapping studies of the reaction of the sulfate radical anion with N1-substituted pyrimidine bases. Comparison with continuous-flow electron paramagnetic resonance experiments. J Chem Soc Perkin Trans 2 1995;12:2153–2162.
[23] Staško A, Polovka M, Brezová V, Biskupič S, Malík F. Tokay wines as scavengers of free radicals (an EPR study). Food Chem 2006;96:185–196.
[24] Staško A, Liptáková M, Malík F, Mišík V. Free radical scavenging activities of white and red wines: an EPR spin trapping study. Appl Magn Reson 2002;22:101–113.
[25] Staško A, Brezová V, Liptáková M, Šavel J. Thermally initiated radical reactions of $K_2S_2O_8$: EPR spin trapping investigations. Magn Reson Chem 2000;38:957–962.
[26] Davies MJ, Gilbert BC, Stell JK, Whitwood AC. Nucleophilic substitution reactions of spin adducts. Implications for the correct identification of reaction intermediates by EPR/spin trapping. J Chem Soc Perkin Trans 2 1992;3:333–335.
[27] Clément JL, Gilbert BC, Ho WF, Jackson ND, Newton MS, Silvester S, Timmins GS, Tordo P, Whitwood AC. Use of a phosphorylated spin trap to discriminate between the hydroxyl radical and other oxidising species. J Chem Soc Perkin Trans 2 1998;8:1715–1717.
[28] Timmins GS, Liu KJ, Bechara EJH, Kotake Y, Swartz HM. Trapping of free radicals with direct in vivo EPR detection: a comparison of 5,5-dimethyl-1-pyrroline-N-oxide and 5-diethoxyphosphoryl-5- methyl-1-pyrroline-N-oxide as spin traps for $HO^{\bullet}$ and $SO_4^{\bullet-}$. Free Radic Biol Med 1999;27:329–333.
[29] Rapta P, Polovka M, Zalibera M, Breierová E, Žitňanová I, Márová I, Čertík M. Scavenging and antioxidant properties of compounds synthesized by carotenogenic yeasts stressed by heavy metals—EPR spin trapping study. Biophys Chem 2005;116:1–9.
[30] Brindzová L, Čertík M, Rapta P, Zalibera M, Mikulajová A, Takácsová M. b Antioxidant activity, β-glucan and lipid contents of oat varieties. Czech J Food Sci 2008;26: 163–173.
[31] Mikulajová A, Takácsová M, Rapta P, Brindzová L, Zalibera M, Nemeth K. Total phenolic contents and antioxidant capacities of cereal and pseudocereal genotypes. J Food Nutr Res 2007;46:150–157.
[32] Moore J, Yin JJ, Yu L. Novel fluorometric assay for hydroxyl radical scavenging capacity (HOSC) estimation. J Agric Food Chem 2006;54:617–626.
[33] Wardman P. Reduction potentials of one-electron couples involving free-radicals in aqueous-solution. J Phys Chem Ref Data 1989;18:1637–1755.
[34] Staško A, Brezová V, Biskupič S, Mišík V. The potential pitfalls of using 1,1-diphenyl-2-picrylhydrazyl to characterize antioxidants in mixed water solvents. Free Radic Res 2007;41:379–390.
[35] Duling DR. Simulation of multiple isotropic spin-trap EPR-spectra. J Magn Reson B 1994;104:105–110.
[36] Eberson L, Persson O. Generation of acyloxyl spin adducts from N-tert-butyl-α-phenylnitrone (PBN) and 4,5-dihydro-5,5-dimethylpyrrole 1-oxide (DMPO) via nonconventional mechanisms. J Chem Soc Perkin Trans 2 1997;1689–1696.
[37] Rosen GM, Beselman A, Tsai P, Pou S, Mailer C, Ichikawa K, Robinson BH, Nielsen R, Halpern HJ, MacKerell AD. Influence of conformation on the EPR spectrum of 5,5-dimethyl-1-hydroperoxy-1-pyrrolidinyloxyl: a spin trapped adduct of superoxide. J Org Chem 2004;69:1321–1330.
[38] Clement JL, Ferre N, Siri D, Karoui H, Rockenbauer A, Tordo P. Assignment of the EPR spectrum of 5,5-dimethyl-1-pyrroline N-oxide (DMPO) superoxide spin adduct. J Org Chem 2005;70:1198–1203.
[39] Dikalov S, Jiang JJ, Mason RP. Characterization of the high-resolution ESR spectra of superoxide radical adducts of 5-(diethoxyphosphoryl)-5-methyl-1-pyrroline N-oxide (DEPMPO) and 5,5-dimethyl-1-pyrroline N-oxide (DMPO). Analysis of conformational exchange. Free Radic Res 2005;39:825–836.
[40] Rockenbauer A, Clement JL, Culcasi M, Mercier A, Tordo P, Pietri S. Combined ESR and thermodynamic studies of the superoxide adduct of 5-(diethoxyphosphoryl)-5-methyl-1-pyrroline N-oxide (DEPMPO): hindered rotation around the O-O bond evidenced by two-dimensional simulation of temperature-dependent spectra. J Phys Chem A 2007;111:4950–4957.
[41] Padmaja S, Alfassi ZB, Neta P, Huie RE. Rate constants for reactions of $SO_4^{\bullet-}$ radicals in acetonitrile. Int J Chem Kinet 1993;25:193–197.
[42] Wu G, Yosuke Katsumura Y, Chub G. Photolytic and radiolytic studies of $SO_4^{\bullet-}$ in neat organic solvents. Phys Chem Chem Phys 2000;2:5602–5605.
[43] Ivanov KL, Glebov EM, Plyusnin VF, Ivanov YuV, Grivin VP, Bazhin NM. Laser flash photolysis of sodium persulfate in aqueous solution with additions of dimethylformamide. J Photochem Photobiol A 2000;133:99–104.
[44] Davies MJ. Recent developments in EPR spin-trapping. In: BC Gilbert, JM Davies, DM Murphy, KA McLauchlan, editors. Electron paramagnetic resonance. Volume 18, Electron paramagnetic resonance, specialist periodical reports. Cambridge: Royal Chemical Society; 2002. p 47–73.
[45] Tordo P. Spin-trapping: recent developments and applications. In: NM Atherton, BC Gilbert, JM Davies, editors. Electron paramagnetic resonance. Volume 16, Electron paramagnetic resonance, specialist periodical reports. Cambridge: Royal Chemical Society; 1998. p 116–144.
[46] Culcasi M, Rockenbauer A, Mercier A, Clément JL, Pietri S. The line asymmetry of electron spin resonance spectra as a tool to determine the cis:trans ratio for spin-trapping adducts of chiral pyrrolines N-oxides: the mechanism of formation of hydroxyl radical adducts of EMPO, DEPMPO, and DIPPMPO in the ischemic-reperfused rat liver. Free Radic Biol Med 2006;40:1524–1538.
[47] Roginsky V, Lissi EA. Review of methods to determine chain-breaking antioxidant activity in food. Food Chem 2005;92:235–254.
[48] Antolovich M, Prenzler PD, Patsalides E, McDonald S, Robards K. Methods for testing antioxidant activity. Analyst 2002;127:183–198.
[49] Zang LY, Cosma G, Gardner H, Castranova V, Vallyathan V. Effect of chlorogenic acid on hydroxyl radical. Mol Cell Biochem 2003;247:205–210.
[50] Brezová V, Šlebodová A, Staško A. Coffee as a source of antioxidants: an EPR study Food Chem 2009;114:859–868. doi:10.1016/j.foodchem.2008.10.025
[51] Rice-Evans CA, Miller NJ, Paganga G. Structure-antioxidant activity relationships of flavonoids and phenolic acids. Free Radic Biol Med 1996;20:933–956.

This paper was first published online on iFirst on 8 April 2009.

Supplementary Figures

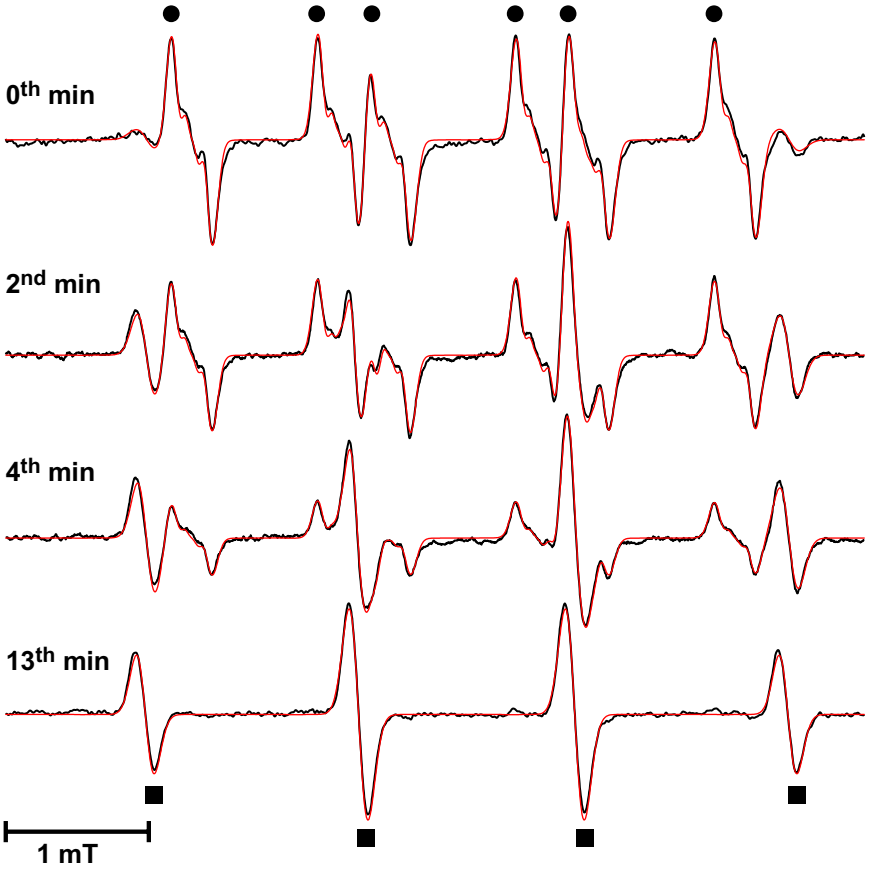

Figure S1. EPR spectra (black lines) with the corresponding simulation (red lines) detected 0, 2, 4 and 13 min after mixing 200 μL of water with 20 μL of reaction mixture containing 1 mM $K_2S_2O_8$ and 20 mM DMPO in DMSO, that was incubated for 30 min at 333 K before mixing: (●) $^{\bullet}$DMPO-$SO_4^{\bullet-}$, (■) $^{\bullet}$DMPO-OH; microwave power, 10 mW; modulation amplitude, 0.1 mT).

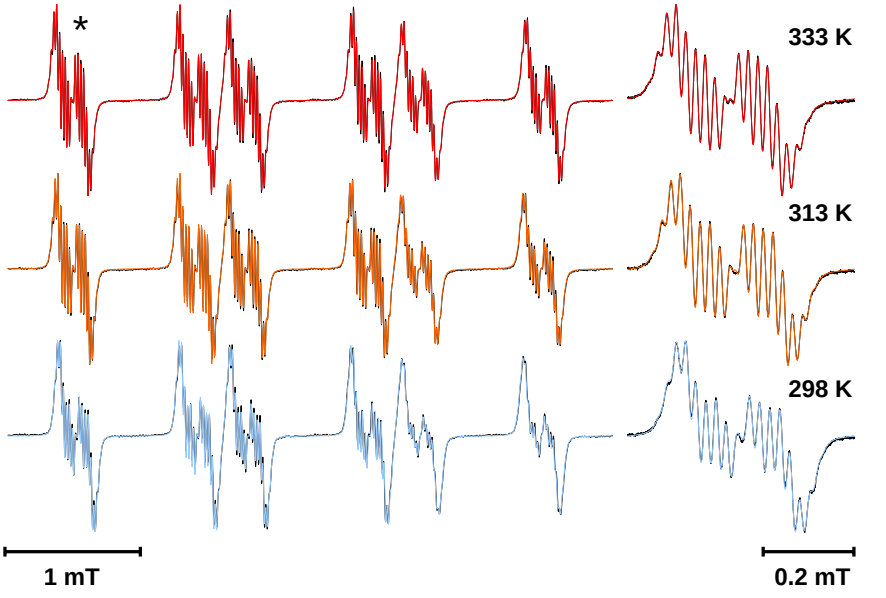

Figure S2. EPR spectra (black lines) and the corresponding computer simulations (coloured lines) of the $^{\bullet}$DMPO-$SO_4^{\bullet-}$ adduct obtained for argon-saturated 1 mM $K_2S_2O_8$ and 20 mM DMPO in DMSO at noted temperatures, after 20 min pre-incubation at 333 K: microwave power, 1 mW; field modulation, 0.005 mT; line marked by * is expanded in the right part; for the hyperfine coupling constants see Table I.

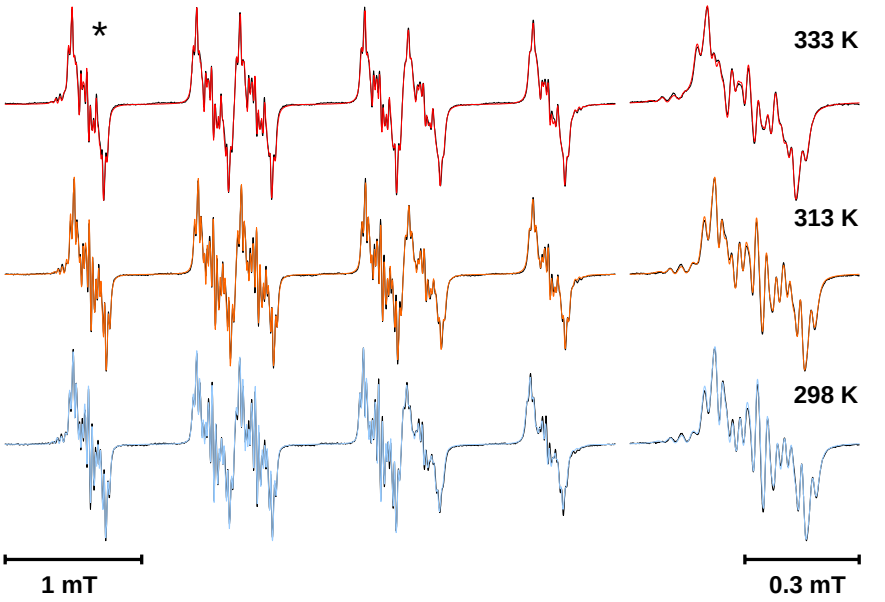

Figure S3. EPR spectra (black lines) and the corresponding computer simulations (coloured lines) of the $^{\bullet}$EMPO-SO_4^- adduct obtained for argon-saturated 1 mM $K_2S_2O_8$ and 20 mM EMPO in DMSO at noted temperatures, after 20 min pre-incubation at 333 K: microwave power, 1 mW; field modulation, 0.005 mT; line marked by * is expanded in the right part; for the hyperfine coupling constants see Table I.

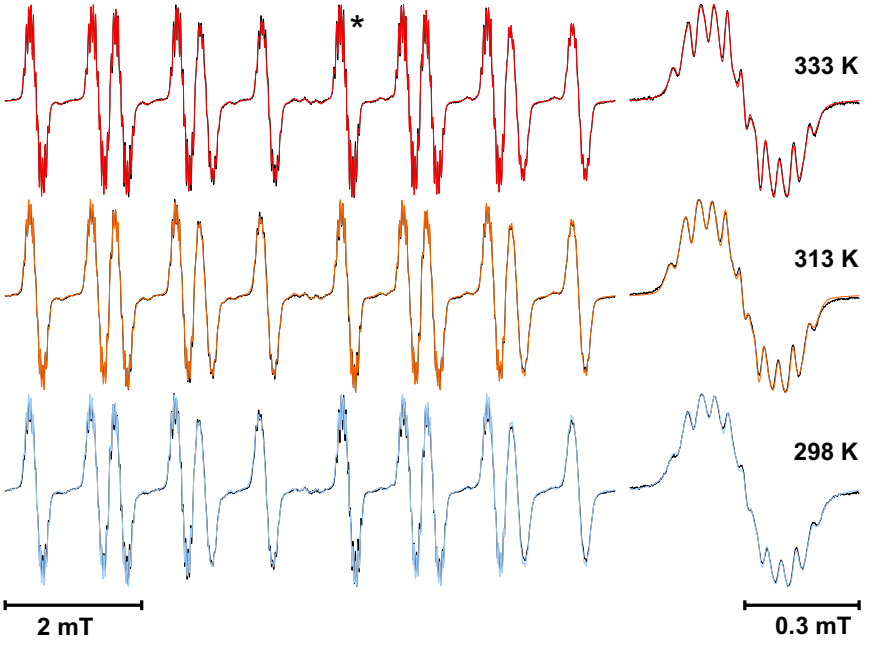

Figure S4. EPR spectra (black lines) and the corresponding computer simulations (coloured lines) of the $^{\bullet}$DIPPMPO-SO_4^- adduct obtained for argon-saturated 1 mM $K_2S_2O_8$ and 20 mM DIPPMPO in DMSO at noted temperatures, after 20 min pre-incubation at 333 K: microwave power, 1 mW, field modulation, 0.01 mT; line marked by * is expanded in the right part; for the hyperfine coupling constants see Table I.

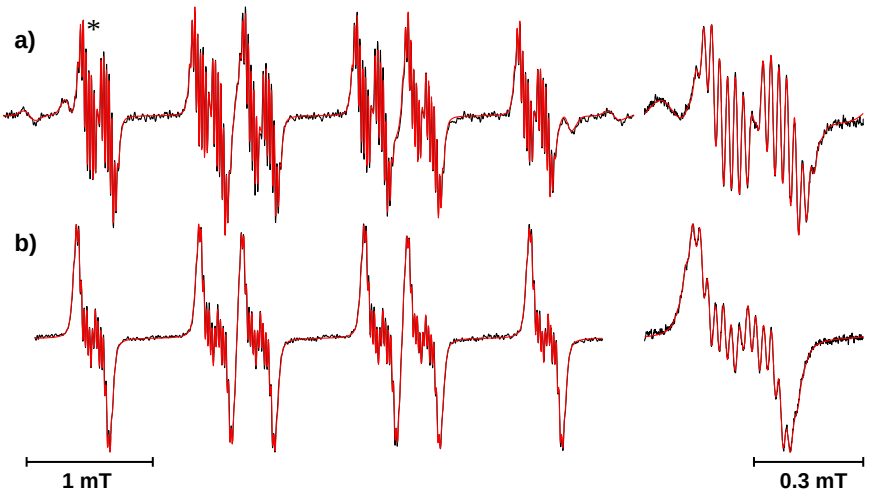

Figure S5. EPR spectra (black lines) and the corresponding computer simulations (red lines) of a) $^{\bullet}$DMPO-SO_4^- (84%), $^{\bullet}$DMPO-OR (13%) and $^{\bullet}$DMPO-R (3%) adducts obtained for argon-saturated 1 mM $K_2S_2O_8$, 80 mM DMPO in DMF after 20 min at 333 K; b) $^{\bullet}$DMPO-SO_4^- adduct obtained for argon-saturated 1 mM $K_2S_2O_8$, 20 mM DMPO in 95% ACN/water (v/v) after 20 min at 333 K: microwave power, 1 mW, field modulation, 0.01 mT; line marked by * is expanded in the right part; for the hyperfine coupling constants see Table II.

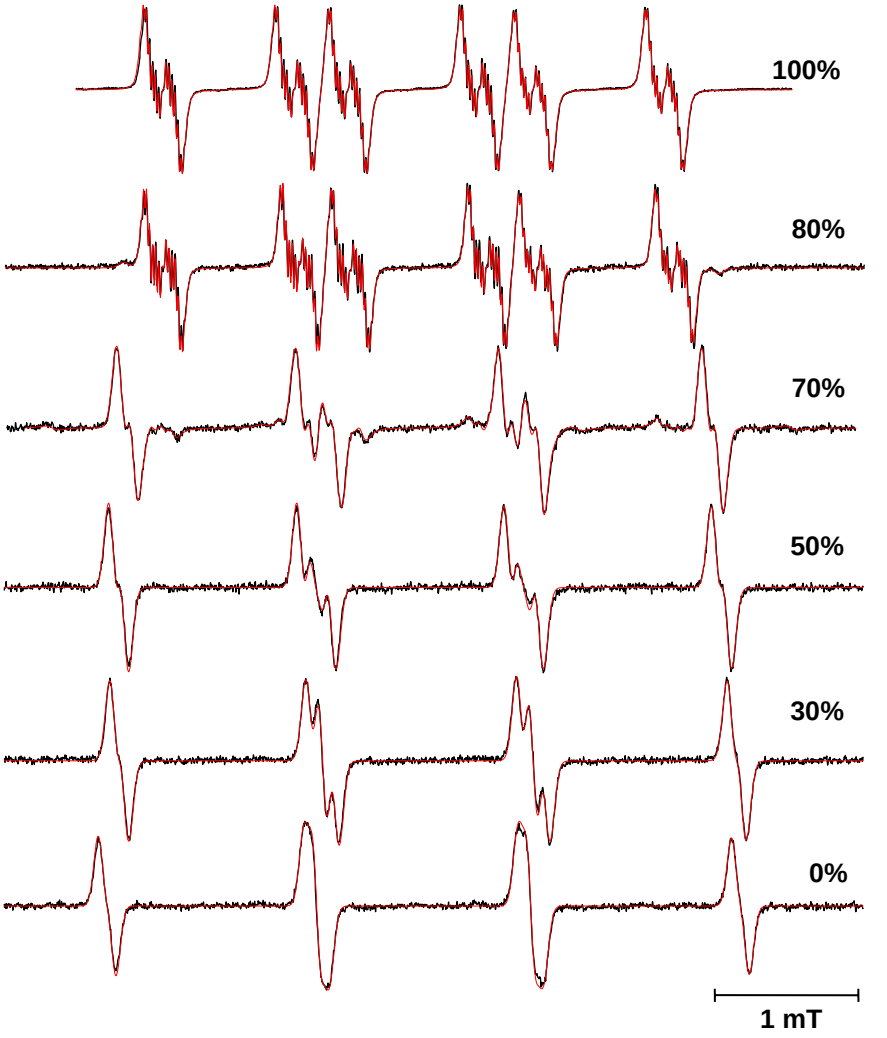

Figure S6. EPR spectra obtained at 20th min in 1 mM $K_2S_2O_8$ and 20 mM DMPO argon-saturated solutions with noted DMSO/water ratios (v/v) at 333 K (solid lines) (microwave power, 10 mW, field modulation, 0.005 mT for 100 & 80% DMSO, 0.02 mT for the rest) with corresponding computer simulations (red lines).

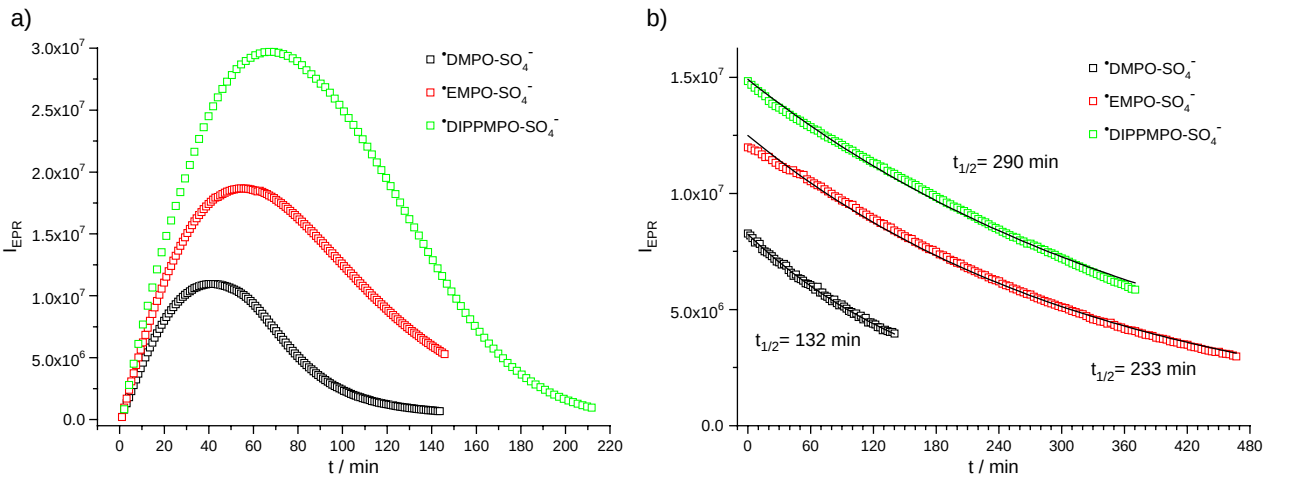

Figure S7. a) Evolution of the EPR signal integral intensity (I_{EPR}) for sulphate radical adducts in 1 mM $K_2S_2O_8$ and 20 mM DMPO or EMPO or DIPPMPO argon-saturated DMSO solutions at 333 K; b) decay of the sulphate radical adduct EPR signal at 298K together with the fitted pseudo-first order kinetic curves and half-lives; (microwave power, 10 mW, field modulation, 0.1 mT).